Deviations from the Stress−Optical Rule in Telechelic Associative Polymer Solutions

Linda Pellens,† Jan Vermant, and Jan Mewis*

Department of Chemical Engineering, K.U. Leuven, W. de Croylaan 46, B-3001 Leuven, Belgium

Received November 12, 2004; Revised Manuscript Received December 24, 2004

ABSTRACT: The stress−optical rule is known to be valid for a wide range of polymeric fluids, as long as the chains are only slightly extended. In solutions of associative polymers, strain hardening and shear thickening are known to occur, and non-Gaussian chain stretching has been proposed as an explanation for these phenomena. Hence, the stress−optical rule could be expected to break down for these materials. Here, a rheooptical investigation of a telechelic associative polymer is presented. Various nonlinear flow fields have been applied. When strain hardening or shear thickening occurs, it is shown that the stress−optical rule is indeed not valid anymore. An analysis of the rather small values of the strains at the onset of the nonlinearities suggests that the bridging chains are probably in a stretched state even in the absence of flow. On the other hand, the birefringence data indicate that the local deformation of the polymeric chains is more complex. The final result is that the mechanical behavior can be described quite well by a transient network model, assuming initially strained chains. The rheooptical data, however, prove that the actual structural changes in associative polymers are even more complex, possibly because of the presence of micelles.

1. Introduction

Telechelic associative polymers typically consist of a hydrophilic backbone with hydrophobic groups grafted at the ends of the chain, although the reverse is also possible.[1,2] When dissolved in an aqueous medium at moderate concentrations, these polymers are assumed to form flowerlike micelles with an inner hydrophobic core and an outer corona of hydrophilic chains arranged into loops. At higher concentrations, bridges are formed between the micelles, and a transient network structure develops.[1]

The steady-state shear rheology of telechelic associative polymers displays, at sufficiently high concentrations, some specific features.[1,3−5] Typically, a Newtonian region is observed at low shear rates. The Newtonian viscosity is described on the basis of a transient network. The magnitude of that viscosity depends on the kinetics of attachment and detachment of the hydrophobic groups; these associate in micelles which constitute the actual network junctions. A shear thickening region often develops at intermediate shear rates. In some cases a shear thinning region can be detected at the highest shear rates,[4] but often flow instabilities arise before this region is reached.[3,6−8] The occurrence of shear thickening in these systems has been attributed to two different mechanisms. Shear-induced transitions from intra- to intermicellar associations have been suggested by some authors.[9−11] Alternatively, non-Gaussian stretching of the chains has been invoked to explain this behavior.[4,12,13]

Although shear thickening is quite common in telechelic polymers, it is not a universal characteristic of associative behavior. Other rheological features have been identified that seem to be more general characteristics of the entire class of associative polymers, including the nontelechelic ones.[5] One of these features is a peculiar strain dependence of the stress relaxation modulus. The instantaneous modulus initially rises with increasing strain. At somewhat higher strains, the long time part of the relaxation function starts to decrease; this decrease then systematically propagates to shorter times. Note that the strain hardening at short times is observed already at low values of the strain ($\gamma \cong 0.1$). The strain hardening seems to reflect a non-Gaussian stretching of the chains, caused by the relatively strong hydrophobic links. The kinetics of attachment and detachment of these links govern the relaxation behavior at longer times. Hence, nonlinear relaxation experiments provide the means to separate the effects of the nonlinear forces in the chains from those of the kinetics of the network. If the strain could be applied on a time scale that is shorter than that of the relaxation kinetics of the network, the forces that result from nonlinear chain stretching could be studied without the interference of the kinetics of attachment and detachment.

Techniques to detect the optical properties have been combined successfully with rheological measurements to determine structural changes during flow in various complex fluids.[14] In polymers, the optical and mechanical properties are closely related. Under suitable conditions the birefringence is proportional to the stress. This is expressed by the stress−optical rule (SOR), which for the shear stress σ_{xy} gives the following expression:[14]

$$\sigma_{xy} = \frac{1}{2C}\Delta n' \sin 2\chi \tag{1}$$

where C is the stress−optical coefficient, $\Delta n'$ the birefringence, and χ the orientation angle of the principal directions of the refractive index tensor with respect to the main axes of the shear flow. This expression is valid for relatively small values of the end-to-end vector and does not take into account form birefringence; i.e., in solution the refractive indices of polymer and solvent should be matched. When the polymer chains are stretched outside the Gaussian region, the stress and birefringence will increase in a different manner: the stress will diverge at full stretching whereas the bire-

† Current address: Procter & Gamble European Technical Centre, Temselaan 100, B-1853 Strombeek-Bever, Belgium.

* Corresponding author: e-mail jan.mewis@cit.kuleuven.ac.be.

10.1021/ma047672k CCC: $30.25
Published on Web 02/03/2005

fringence will not. This has e.g. been observed during elongational flow experiments on polymer melts and solutions.[15,16] In these cases the critical strain rate $\dot{\epsilon}_0$ for the onset of deviations to the SOR is predicted to be of the order of the reciprocal Rouse time τ_R:[15]

$$\dot{\epsilon}_0 \tau_R > 1 \tag{2}$$

The subsequent critical stresses are of the order of 10^6 Pa for polymer melts and 10^4 Pa for polymer solutions.[16] Hence, for normal polymer melts or solutions it is difficult to achieve these high levels of stretching in standard shear rheometers.

Few studies have dealt with probing the rheooptical properties of associative polymer solutions. Chassenieux et al.[13] reported stretching of telechelic ionomers under shear. In these measurements the birefringence strongly increased at the onset of shear thickening, reflecting strong chain stretching. These authors concluded that the stress−optical rule was obeyed in all regions. Le Meins et al.[8,17] examined the optical behavior of HEUR polymers (hydrophobicallly modified ethoxylated urethanes). The rheooptical results were used to attribute the observed flow instabilities at high shear rates to shear-induced phase separation. Le Meins[18] also reported small deviations from the stress−optical rule for a HEUR with MW = 20 000 and C16 hydrophobes at high shear rates.

The present rheooptical investigation was triggered by the observation that strain hardening started at relatively small strains as well as by the results of some model validation.[19,20] A transient network model was found to describe the nonlinear rheological behavior of telechelic polymers quite well, at least qualitatively. The strains and strain rates at the onset of the nonlinear behavior were, however, systematically overestimated by at least an order of magnitude. The highly nonlinear behavior of the telechelic associative polymers suggests that some aspects of the microstructure are not incorporated in the available network models. Here, the rheooptical behavior of telechelic associative polymers will be examined during different types of flows to elucidate the physical mechanisms that govern the nonlinear rheological behavior of the materials under consideration.

2. Materials and Methods

2.1. Materials. The HEUR polymers that are being used here as telechelic associative polymers consist of a poly(ethylene oxide) backbone, modified at its chain ends with hydrophobic groups via urethane spacers. The samples have been synthesized according to a procedure described in the literature.[18,21] They contain PEO chains with a molecular weight of 20 000 and C18 hydrocarbon hydrophobes at the chain ends. The percentage of chain ends modified with C18 hydrophobes was found to be 88%, as determined with ^{1}H NMR.[18] Solutions were prepared by gently mixing the polymer powder with deionized, twice-distilled water for at least 48 h and letting the sample recover for at least 24 h. The rheology of these solutions has been discussed elsewhere.[5,19,22]

2.2. Methods. The mechanical and rheooptical measurements have been performed on an MCR300 rheometer (Paar Physica, Austria) (see Figure 1). A Couette cell was used as flow geometry; in this manner the velocity/velocity gradient plane could be probed in the rheooptical measurements. The inner and outer radii, respectively 16.95 and 17.95 mm (R_i/R_o = 0.94), have been chosen to accommodate the laser beam. The height of the cylinder is 16.6 mm. End effects on the measured stresses are estimated to be around 10%, using the method described by Macosko.[23] The effect of the ends on the optical data is negligible as the aspect ratio of the Couette cell (33.2) is sufficiently high.[24] The temperature can be controlled by means of a thermal jacket; all experiments were carried out at 20.0 ± 0.1 °C. The use of a rheometer for rheooptical measurements provides an opportunity to apply different kinds of well-defined flow fields in these measurements. It also allows to measure simultaneously the optical and rheological properties.

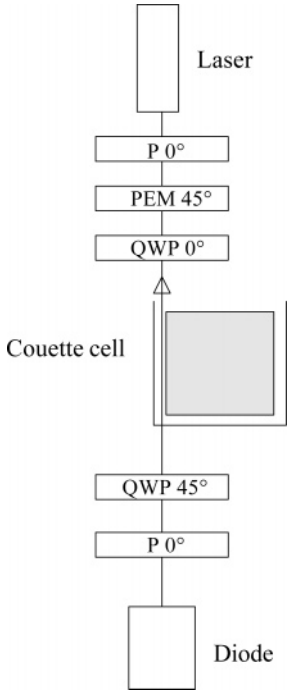

Figure 1. Experimental setup (P = polarizer, PEM = photoelastic modulator, QWP = quarter wave plate).

The optical part of the setup consists of a polarization state generator (PSG) and a polarization state analyzer (PSA) positioned respectively before and after the flow cell. The system operates with a He−Ne laser (10 mW, Uniphase, $\lambda \cong$ 632 nm). As a PSG, a Glan-Thompson polarizer at 0° is placed before a feedback-stabilized photoelastic modulator (PEM, Beaglehole Instruments, New Zealand). A zero-order quarter wave plate is inserted at 0° after the PEM (Figure 1). In the PEM an oscillatory stress induces an oscillatory birefringence. This produces a retardation δ'_{PEM}:

$$\delta'_{PEM} = A \sin \Omega t \tag{3}$$

where A is the amplitude and Ω the frequency (50 kHz) of the oscillating birefringence of the PEM. With this high-frequency modulation fast transient phenomena can be followed. An optical filter is placed before the sample to adapt the intensity of the light to the sensitivity range of the measurement diode. A set of two quartz prisms is used to direct the light beam through the sample without altering the polarization state of the light. The PSA consists of a quarter wave plate oriented at 45° and a Glan-Thompson polarizer at 0°. The intensity of the light is measured using a sensitive diode (Beaglehole Instruments) in combination with a fast, 12 bit data acquisition card (National Instruments NI 6033), which allows millisecond resolution. When a purely birefringent sample is measured, the intensity of the light that is detected by the diode can be calculated, using the appropriate Müller matrices:[14]

$$I = \frac{I_0}{4}[1 - (J_0(A) + 2J_2(A)2\cos \Omega t) \sin 2\chi \sin \delta' + (2J_1(A) \sin \Omega t) \cos 2\chi \sin \delta'] \tag{4}$$

where J_m are Bessel functions of the mth order. The amplitude

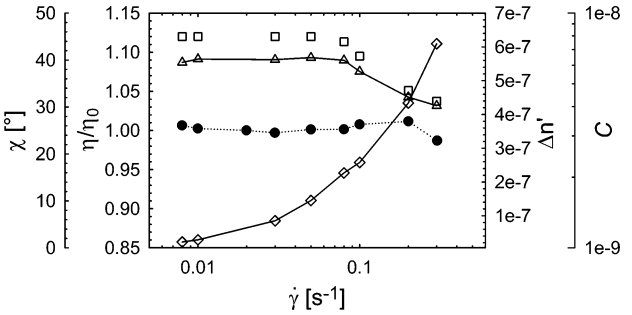

Figure 2. Steady-state shear data of viscosity (●), birefringence $\Delta n'$ (◇), stress−optical coefficient C (△), and orientation angle χ (□) for sample 20k-C18 at 2.4 wt %.

A of the PEM is controlled to have $J_0(A) = 0$. No linear dichroism was detected at the velocities and concentrations used; hence, it can be ignored in the further analysis. By using lock-in amplifiers (SR830, SRI) the first and second harmonic of the signals are extracted. When the amplitudes of the harmonics are divided by the dc signal, the following equations can be used to compute the orientation angle and birefringence (see e.g. ref 25):

$$R_1 = 2J_1(A) \cos 2\theta \sin \delta' \tag{5}$$

$$R_2 = -2J_2(A) \sin 2\theta \sin\delta' \tag{6}$$

$$\theta = \frac{1}{2} \arctan\left(-\frac{J_1(A)R_2}{J_2(A)R_1}\right) \tag{7}$$

$$\delta' = \arcsin\left(\frac{1}{2}\sqrt{\left(\frac{R_1}{J_1(A)}\right)^2 + \left(\frac{R_2}{J_2(A)}\right)^2}\right) \tag{8}$$

$$\Delta n' = \lambda\delta'/2\pi d \tag{9}$$

3. Results

3.1. Steady-State Flow. Figure 2 shows the steady-state viscosity data, scaled with the zero-shear viscosity, for a 2.4 wt % sample of the 20k-C18 HEUR polymer. After a Newtonian region, a slight shear thickening region is observed. Only a few data points are available in the subsequent shear thinning region due to the occurrence of flow instabilities, as mentioned above. Figure 2 also contains the birefringence data ($\Delta n'$) at the same flow conditions. To provide a more accurate picture of possible deviations from the stress−optical rule (eq 1), the ratio $\Delta n' \sin 2\chi/2\sigma_{xy}$ ($= C$) is presented, rather than a plot of σ_{xy} vs $\Delta n' \sin 2\chi$. At low shear rates, the value of C is about 6×10^{-9}, which is higher than the values reported for the stress−optical coefficient of regular PEO solutions[25] for which the coefficients are of the order of 1×10^{-9}. The latter solutions obey the SOR in shear flow, in contrast with the shear rate dependence that is observed here. For the system used in Figure 2, the value of the stress−optical coefficient starts to drop already in the shear thickening region. The orientation angle χ is shown in the same graph.

3.2. Large-Amplitude Oscillatory Flow. The polymer solutions were also subjected to oscillatory experiments at constant frequency with varying amplitude. When increasing the peak strain, strain hardening behavior is known to occur in these systems.[5,26,27] For a frequency of 5 rad/s the evolution of various moduli with peak strain is shown in Figure 3. The evolution of the stress−optical coefficient is also included in the figure. As the strain increases, C decreases below its

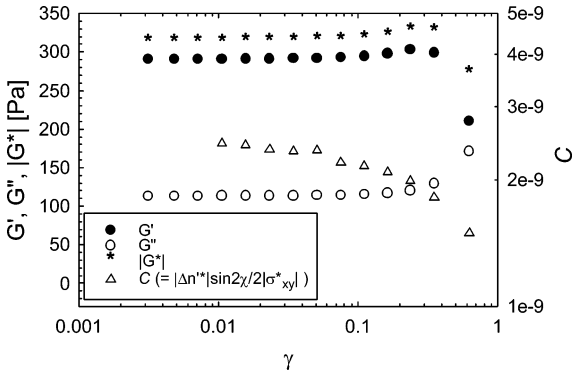

Figure 3. Rheooptical dynamic data at a frequency of 5 rad/s and at different strain amplitudes for sample 20k-C18 at 2.4 wt %.

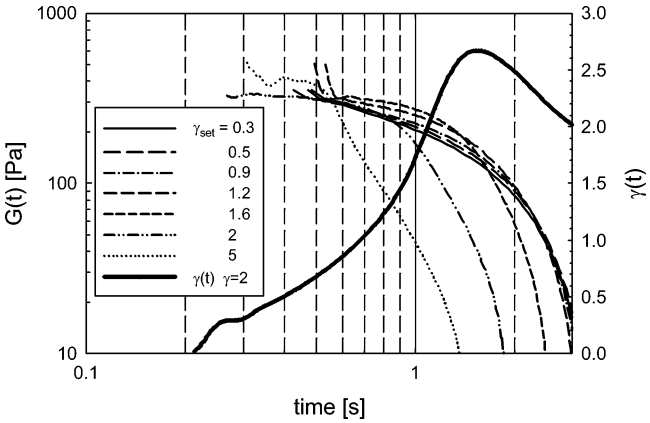

Figure 4. Nonlinear moduli for a 2.4 wt % 20k-C18 HEUR sample at different set strain values in nominal step strain experiments.

low strain limit of 2.5×10^{-9}. This low strain limit of C is smaller than in steady shear flow. It is a decreasing function of frequency. At 10 rad/s it becomes 1.5×10^{-9}, whereas at 1 rad/s, i.e., near the relaxation frequency, it reaches the value obtained in the steady-state experiments.

3.3. Stress−Strain Experiments. A relevant experiment to test the chain stretch and deformation is to perform stress−strain experiments. Figure 4 shows the response of an associative polymer to a rapidly applied deformation for different values of the set strain. This is nominally a step-strain experiment, but in the setup used, it takes a substantial amount of time to reach the set strain. Therefore, the procedure can be used to analyze stress−strain curves. The device is stress-controlled, and therefore a coupling occurs between the instrumental inertia and the elasticity of the material, known as viscoelastic ringing.[28] It renders the evolution of the strain as a function of time nonmonotonic, as illustrated in Figure 4 for a set strain value of 2. As a result of the viscoelastic ringing, the applied strain shows an overshoot, which causes the flow and stress to change direction after about 3 s. This complex strain evolution, however, does not interfere with the present analysis of nonlinear chain stretching, as only data pertaining to the initial part of the deformation will be used.

Although the strain evolves in a complex manner as a function of time, all the characteristic features of the response of an associative polymer to a step strain are present in Figure 4: strain hardening of the moduli at

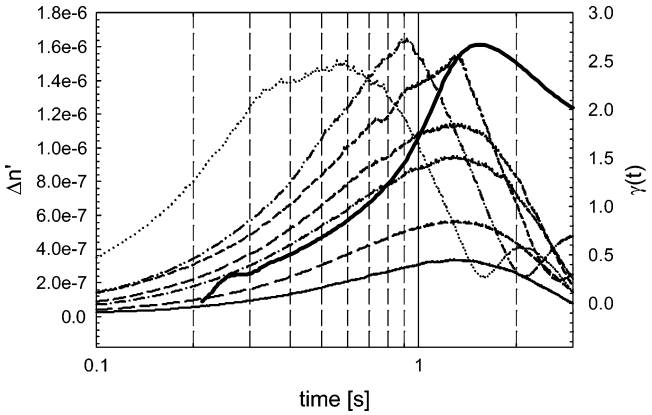

Figure 5. Evolution of the birefringence with time in nominal step-strain experiments at different set strain values (sample and symbols as in Figure 4).

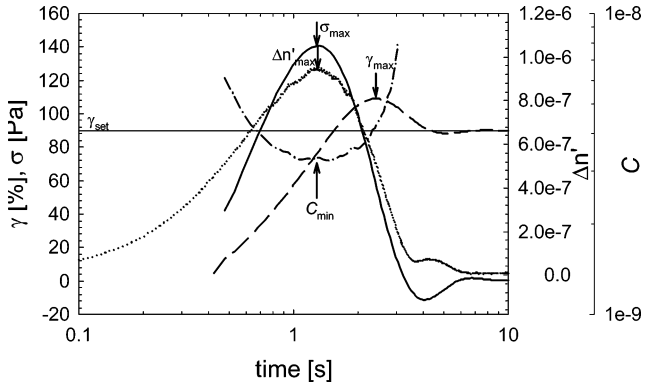

Figure 6. Stress σ_{xy} (—), strain γ (– –), birefringence $\Delta n'$ (• • •), and the stress–optical coefficient C (– • –) as a function of time during a nominal step-strain experiment, applied strain = 0.9.

short times and the characteristic drop of the relaxation function at longer times.[5] Figure 5 shows the corresponding evolution of the birefringence. The maximum in the birefringence curves shifts to large values with the total applied strain, but at the highest strains ($\gamma = 5$) a rather abrupt transition is observed from increasing to decreasing peak birefringence.

A comparison of the evolution of the stress and the birefringence with time during an experiment with a set strain value of 0.9 is shown in Figure 6. The stress (σ_{xy}) and birefringence ($\Delta n'$) curves follow a similar evolution; they both reach their maximum value at the same time as indicated by the arrows. This does, however, not coincide with the maximum of the strain which occurs much later. The same figure also shows the evolution of the ratio between birefringence and stress. As long as stress and birefringence increase, the stress–optical coefficient decreases, being always lower than its zero shear value. It can be concluded that in this type of experiment the stress–optical rule is also violated. Once the stress and birefringence start to decrease again, the value of C rises, growing beyond the zero shear value because of the flow reversal resulting from the overshoot in the strain.

To examine the effect of non-Gaussian chain stretching on the ratio of stress over birefringence, the evolution of σ_{xy}/γ with strain is examined. As indicated earlier, to probe the nonlinear response of the network only data should be used in which junction detachment did not interfere yet with non-Gaussian straining. To

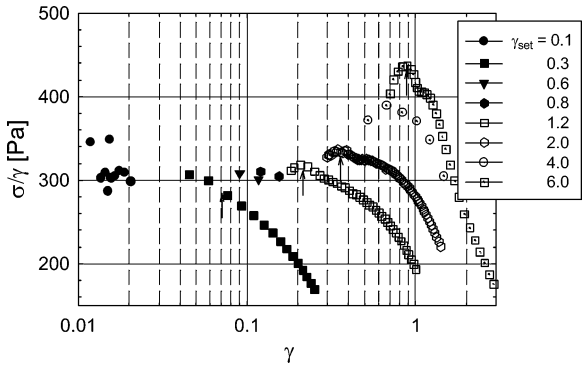

Figure 7. Stress/strain ratio for different set strain values (2.4 wt % of 20k-C18); arrows indicate up to which point data are used in the further analysis.

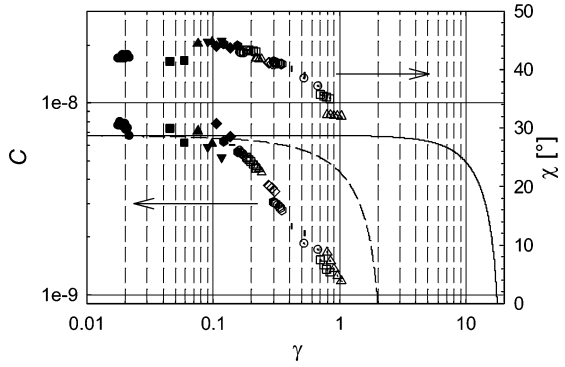

Figure 8. Stress–optical coefficient for different strains in nominal step-strain experiments (sample and symbols as in Figure 7). Lines represent predictions using the normal nonlinear theory of rubber elasticity (—) and assuming an initial stretching of $5.4R_0$ (– –).

determine which part of the deformation curve satisfies this condition, the stress–strain curves for experiments at different set values of the strain can be compared. In these experiments, the peak strain occurs at roughly the same time, and hence the strain rate increases with increasing set strain value. Hence, as long as the network persists, the same stresses should occur in the chains at the same strains, irrespective of the set strain value. Figure 7 shows the ratio of stress over strain, plotted vs strain, in experiments with different set strain values. For reasons of clarity not all data points are shown.

The initial parts of the curves superimpose indeed. The faster the strain rate, the longer the common curve is followed; the latter is described by the envelope of the various curves in Figure 7. Its steep rise is proof of a pronounced strain hardening in the network chains, which can be attributed to non-Gaussian chain stretching. The resulting ratio of the birefringence over the stress is plotted in Figure 8. The stress–optical coefficient is only constant up to strains of ≅0.15. Above this strain, the value of the stress–optical coefficient steadily decreases with increasing strain. The evolution of the orientation angle is also shown in Figure 8. It can be seen that the stress–optical coefficient starts to decrease as soon as the orientation angle starts to deviate from 45°.

4. Discussion

4.1. Non-Gaussian Chains. As is shown in Figure 2, the stress–optical coefficient in steady shear flow

decreases upon reaching the shear thickening zone; the stress−optical rule is already violated in that flow regime. The stress−optical rule, as written in eq 1, assumes that the orientation distribution of segments in the chains can be regarded as Gaussian and consequently that both birefringence and stress are proportional to the second moment of the end-to-end distance $\langle \mathbf{RR} \rangle$.[14] Additionally, form birefringence is assumed to be negligible. In the shear thickening region, eq 1 does not apply anymore. Nonlinear stretching of the chains would cause the stress to rise faster with shear rate than the birefringence, thus invalidating the stress−optical rule. Although the failure of the SOR in the shear thickening region is consistent with non-Gaussian stretching, it should be noted that the SOR starts to fail already when the orientation angle begins to deviate from its limiting low shear value of 45°. This is the case in steady-state flow as well as in step-strain experiments (Figures 2 and 8).

In large-amplitude oscillatory flow, the stress−optical coefficient decreases with strain (Figure 3). Again, non-Gaussian stretching could be invoked to explain this phenomenon. In addition to the effect of strain amplitude on the stress−optical coefficient, there also is an effect of frequency: the value of the stress−optical coefficient at low strains decreases with increasing frequency. At the same time, the strain at the onset of the nonlinearity is also somewhat smaller in the LAOS experiments ($\gamma_{crit} \cong 0.05$) than in the step-strain experiments ($\gamma_{crit} \cong 0.1$). Whereas the stress increases with frequency in agreement with Maxwellian behavior, the birefringence increases less strongly (Figure 3). Hence, the segments of the chains in the network turn out to be less oriented than expected on the basis of the stress. This suggests a complex deformation of the chains, possibly resulting from the presence of micellar aggregates.

In addition to the intrinsic birefringence, arising from the anisotropy in the segmental polarizability, there is also a possible contribution that is more closely related to the overall shape of the coil. Form birefringence plays a role when there is sufficient contrast between the refractive indices of the solute and the solvent and when the molecular weight of the polymer is rather high. For the present materials, form birefringence effects where estimated using the formula of Copic.[29] In this manner, the contribution of the form birefringence was found to be at most 30% of the total birefringence. A contrast in refractive index could also give rise to form dichroism, which could not be detected here, further supporting the assumption that form birefringence is negligible.

The results of stress−strain experiments confirm the results from the steady-state flow and LAOS experiments. Again the stress−optical coefficient already starts to decrease at relatively small deformations ($\gamma \cong 0.15$), as shown in Figure 8. The faster increase of the stress in comparison with the birefringence also points to the effect of non-Gaussian chain stretching. The possible role of this phenomenon in the failure of the stress−optical rule can be examined quantitatively with the step-strain data. As the junction points in the associative polymer network can be regarded as permanent for the points on the stress envelope in Figure 7, the nonlinear theory of rubber elasticity can be used. Usually, a Warner approximation of the inverse Langevin function is used to express the relation between the force and chain deformation in a chain which is deformed beyond the limits of a Gaussian distribution:[33]

$$\mathbf{F}(\mathbf{R}) = \frac{-3kT}{Nb^2} \frac{\mathbf{R}}{1 - \frac{R^2}{(Nb)^2}} \tag{10}$$

where $\mathbf{R}$ is the end-to-end vector of the chains and R the modulus of $\mathbf{R}$. N and b are the number and length of the Kuhn segments. For a PEO chain with a molecular weight of 20 000 the values are $N \cong 120$ and $b \cong 1.38$ nm.[19] The values for $\mathbf{R}$ needed to calculate the stress with eq 10 at different strains are determined using an equation of change for the normalized distribution function $\psi(\mathbf{R},t)$ of the end-to-end vector $\mathbf{R}$ for the network chains:[20,34]

$$\frac{\partial \psi}{\partial t} = -\frac{\partial}{\partial \mathbf{R}} \cdot (\psi \mathbf{k} \cdot \mathbf{R}) \tag{11}$$

where $\mathbf{k}$ is the velocity gradient. The total stress is calculated from

$$\sigma \sim \langle -\mathbf{FR} \rangle \tag{12}$$

Similar to the force rule, a general expression for the birefringence of non-Gaussian chains can be obtained:[14,35,36]

$$\Delta n' \sim \left\{ 1 - \frac{3\frac{R}{Nb}}{L^{-1}\left(\frac{R}{Nb}\right)} \right\} \tag{13}$$

where L^{-1} denotes the inverse Langevin function. This expression can be approximated by a series expansion containing only even terms:

$$1 - \frac{3\frac{R}{Nb}}{L^{-1}\left(\frac{R}{Nb}\right)} \cong \frac{3}{5}\left(\frac{R}{Nb}\right)^2 + \frac{1}{5}\left(\frac{R}{Nb}\right)^4 + \frac{1}{5}\left(\frac{R}{Nb}\right)^6 \tag{14}$$

which has been found to be numerically accurate to within 1% over the whole range of R/Nb.[36] Using these expressions for the force and the birefringence, the ratio of the stress and birefringence can be calculated in three dimensions, and the xy-component can be compared with the data. This is shown in Figure 8. The Warner spring predicts deviations from the SOR (solid line in Figure 8) but starting at a critical strain of 2, which is much higher than the experimental value of 0.15. Such an overestimation of the critical strain was also obtained when using the transient network model of Vaccaro and Marrucci.[19,20] The latter model is also based on the Warner approximation to describe the forces, but it includes also a description of the kinetics of the network junctions. Using a more accurate description of the force by an inverse Langevin force rule instead of the empirical Warner approximation does not change the critical strain for the onset of deviations. It is obvious that the discrepancy between the predicted and experimental strain values at the onset of nonlinearities is a significant shortcoming in the modeling of the flow behavior of associative polymers.

4.2. Initial Chain Stretching. There are some constraints on the conformation of the active chains

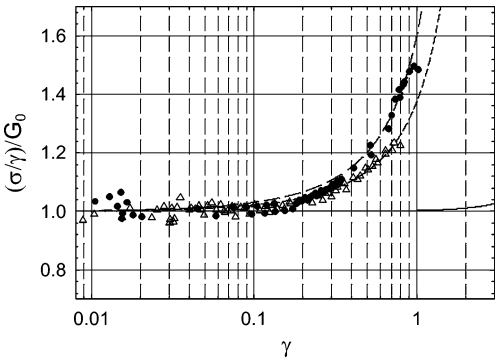

Figure 9. Evolution of the normalized ratio of stress and strain in the step-strain experiments for 2.4 wt % (●) and 2.8 wt % (△) of 20k-C18. Predictions using a normal Warner force rule (—), with $R_i = 5.4R_0$ for 2.4 wt % (– –), and with $R_i = 4.7R_0$ for 2.8 wt % (- -).

constituting the transient network at rest: they have to bridge the distance between the cores of the micelles. In addition, the presence of a corona of loops of hydrophilic chain elements could also interfere with the chain conformation. The net result is that the chains are stretched even at rest, which would amplify the effect of nonlinearities and shift the onset of the deviations from the stress−optical rule to smaller strains. A similar situation occurs in strongly swollen hydrogels; Schröder and Oppermann[37] reported data for the stress and birefringence of such systems. They proposed a quantitative treatment based on non-Gaussian chain statistics with the assumption of affine deformation, which resulted in a deviation from the SOR at low strains. A similar situation could arise in associative polymers. The envelope of the stress−strain curve for the step-strain experiments can be used as a reference. In Figure 9 predictions are shown for the 20k-C18 sample at 2.4 wt % with a regular Warner force rule, starting from relaxed chains. It shows the underestimation of the critical strain as mentioned above. When leaving the initial stretch state of the chains as a fitting parameter, an excellent agreement of data and model is obtained. The required value for the initial end-to-end distance R_i is 5.4 times the equilibrium end-to-end distance R_0 of a free chain. The 2.8 wt % sample will be discussed later.

The value of the initial stretching that is obtained in this manner seems quite large and unrealistic. Some factors, related to the presence of micelles, could contribute to high values of R_i. A rough estimate for the average end-to-end distance of the bridging chains at rest is obtained by calculating the number of micelles in a solution for a given concentration and use this to calculate an average distance between the micellar cores. To perform this calculation, a value for the number of hydrophobic groups in one micelle, i.e., the aggregation number N_{agg}, is required. In general, values for N_{agg} range between 10 and 60 for different associative polymers. There is often a large discrepancy between the results of the different techniques:[38,42,43] values between 15 and 50 have been reported for the polymer investigated here.[44] Average distances d between micellar cores, relative to the equilibrium end-to-end distance R_0, are shown in Table 1. The degree of modification of the 20k-C18 HEUR polymer has been taken into account in these calculations. For the range of N_{agg} reported in the literature, d is found to range from 1.4 to 2.2 R_0. These values clearly show that the bridging chains have to be quite extended in the rest state. They are also in agreement with measurements of the intermicellar distances in different telechelic associative polymers that were performed by François et al.[30] using SAXS and SANS measurements. Their results show that the average distance between micellar cores is larger than the end-to-end distance of a free chain at rest, even when the rheological data clearly indicate that a connected network of micelles is present. For the concentrations of 20k-C18 examined in this work, these authors found an intercore distance of about $2R_0$. The bridging chains can also be hindered in following the affine deformation by the presence of the micelles. In particular, those parts of the chain that are close to the hydrophobic core of the micelles will be restrained from taking up much of the deformation. Hence, the remainder of the chain has to take up more of the deformation, making the effective strain to which that part of the chain is submitted larger than the applied strain. It is hard to quantify the results of having an inhomogeneous deformation of the active chains in the solution.

Table 1. d = Average Distance between Micelle Cores for Different Aggregation Numbers N_{agg}

	N_{agg}	d
2.4 wt %	15	$1.49R_0$
	30	$1.87R_0$
	50	$2.22R_0$
2.8 wt %	15	$1.41R_0$
	30	$1.78R_0$
	50	$2.11R_0$

One way of assessing the assumption of initially stretched chains is to perform the same rheological and rheooptical measurements at different concentrations. The aggregation number density of the micelles does not depend on concentration.[38] Hence, the number of micelles should increase linearly with concentration. This implies that the average distance between the micelles decreases with concentration and hence also the initial stretching of the bridging chains. Figure 9 compares the evolution of the envelope curve of the stress in step-strain experiments at two different concentrations of the 20k-C18 polymer. The critical strain at which the stresses deviate is indeed shifted somewhat to larger strains with increasing concentration: the fitted value of R_i is 4.7 times R_0 for a concentration of 2.8 wt % as compared to 5.4 for 2.4 wt %. This decrease is consistent with a smaller distance between the cores of the micelles, where a larger external strain has to be applied to stretch the intermicellar chains into the non-Gaussian region.

Additional evidence for the effect of micelles on chain stretching is provided by the concentration dependence of the zero-shear viscosity. In several studies[38,45−47] it has been demonstrated that the zero-shear viscosity starts to rise substantially at concentrations well below the overlap concentrations of the micelles. This could be explained on the basis of a sparse network of micelles connected by highly stretched chains. In several DLS studies[38,47] both the hydrodynamic radius of an isolated PEO chain in solution and the hydrodynamic radius of the micelles have been measured or calculated. The results indicate that the hydrodynamic radius of the micelles can be more than twice the hydrodynamic radius of an individual free chain, suggesting substantial stretching of the PEO chains in the corona of the micelles, possibly due to steric effects. This implies that

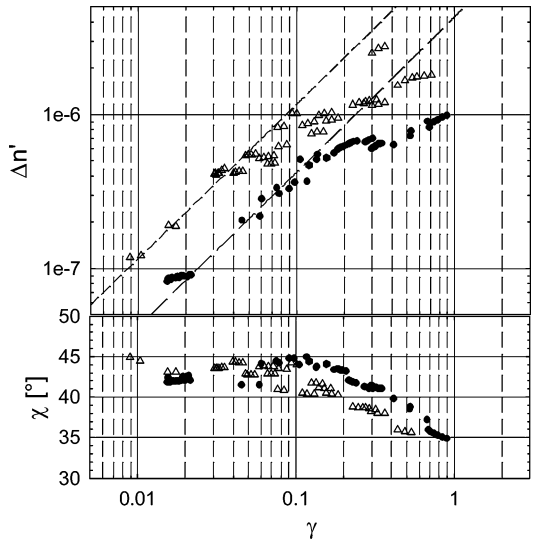

Figure 10. Birefringence and orientation angle for 2.4 wt % (●) and 2.8 wt % (△) in step-strain experiments. Predictions using a Warner force rule with $R_i = 5.4R_0$ for 2.4 wt % (- -) and $R_i = 4.7R_0$ for 2.8 wt % (—).

the chains bridging the micelles have to be stretched as well.

A final remark can be made about the evolution with concentration of the relaxation time of telechelic associative polymers. The fact that the relaxation time rises with concentration of polymer has often been attributed to the existence of so-called superbridges.[1] On the basis of the observations in the present work, however, the dependency of the relaxation time on concentration can also be rationalized by considering the initial stretching of the chains at rest. As the concentration increases, micelles are packed closer, and the stretching of the chains between the micelles will decrease. This would reduce the force in the chains and hence the probability of dissociation of a hydrophobic group from a junction point,[20,48] which is directly related to the relaxation time.

In Figure 8, also predictions for C are shown that are based on the initially stretched state of the chains as derived from the rheological data. The predicted values for the stress−optical coefficient now start to decrease much earlier than the predictions without initially stretched chains but still at larger strains than found experimentally. As the rheological data could be fitted when assuming non-Gaussian chains with the proper degree of prestretching, the failure to describe C indicates that this model does not describe the rheooptical behavior. The measured values of the birefringence in the step-strain experiments are shown in Figure 10 as well as predictions for non-Gaussian chains with or without initially stretched chains.

It can be seen that even the assumption of strongly prestretched chains does not result in a more than linear increase of $\Delta n'$ with strain. The experimental values increase even less than linearly with strain for both concentrations studied. It is obvious that the network chains, notwithstanding the large stresses, do not orient as easily in these systems as in normal polymer networks. Consistent with the results presented above, it seems that the presence of additional structures, i.e. the micellar aggregates, is responsible for the deviations.

5. Conclusions

Rheological and rheooptical techniques have been used to investigate transient network models for telechelic associative polymers. At high shear rates or at large strains, i.e., under conditions where shear thickening or strain hardening is observed in such polymers, the stress−optical rule turns out not to apply. A possible explanation is provided by non-Gaussian stretching of the polymer chains. With sufficiently fast transient measurements the stress−strain behavior of the transient network has been isolated from the kinetic effects of rupture and creation of junctions. In this manner the non-Gaussian nature of the chains could be established. It is much more pronounced than predicted on the basis of the nonlinear theory of rubber elasticity. Assuming that the chains in the network are prestretched, the measured stress−strain behavior could be fitted. The presence of micelles as network junctions makes some degree of prestretching plausible. The actual value that is required to describe the data is, however, quite large.

Whereas non-Gaussian behavior would entail in principle a failure of the stress−optical rule, the deviations that are observed cannot be explained by the nonlinearity derived from the rheological data. Even in the case of strain hardening the birefringence is found to increase less than proportional to the strain. Again the presence of micellar aggregates could explain this effect. It can be concluded that both the rheological and rheooptical data indicate a stronger and more complex deformation of the chains than assumed in normal network theories. The most logical reason for the deviations is the presence of micellar aggregates in solutions of associative polymers. Incorporation of this feature in the transient network models is hampered by a lack of understanding of the detailed structure of the micelles and its effect on the active network chains.

Acknowledgment. The authors are grateful to Prof. G. Marrucci (Univ. of Naples) for stimulating discussions. L. Pellens acknowledges a scholarship from the FWO-Vlaanderen.

References and Notes

(1) Annable, T.; Buscall, R.; Ettelaie, R.; Whittlestone, D. *J. Rheol.* **1993**, *37*, 695.
(2) Winnik, M. A.; Yekta, A. *Curr. Opin. Colloid Interface Sci.* **1997**, *2*, 424.
(3) Pham, Q. T.; Russel, W. B.; Thibeault, J. C.; Lau, W. *Macromolecules* **1999**, *32*, 5139.
(4) Ma, S. O. X.; Cooper, S. L. *Macromolecules* **2001**, *34*, 3294.
(5) Pellens, L.; Gamez-Corrales, R.; Mewis, J. *J. Rheol.* **2004**, *48*, 379.
(6) Sadeghy, K.; James, D. F. *J. Non-Newton. Fluid Mech.* **2000**, *90*, 127.
(7) Berret, J. F.; Séréro, Y. *Phys. Rev. Lett.* **2001**, *8704*, 8303.
(8) Le Meins, J. F.; Tassin, J. F. *Macromolecules* **2001**, *34*, 2641.
(9) Witten, T. A.; Cohen, M. H. *Macromolecules* **1985**, *18*, 1915.
(10) Wang, S. Q. *Macromolecules* **1992**, *25*, 7003.
(11) Tam, K. C.; Jenkins, R. D.; Winnik, M. A.; Bassett, D. R. *Macromolecules* **1998**, *31*, 4149.
(12) Marrucci, G.; Bhargava, S.; Cooper, S. L. *Macromolecules* **1993**, *26*, 6483.
(13) Chassenieux, C.; Tassin, J. F.; Gohy, J. F.; Jerome, R. *Macromolecules* **2000**, *33*, 1796.
(14) Fuller, G. G. *Optical Rheometry of Complex Fluids*; Oxford University Press: New York, 1995.
(15) Venerus, D. C.; Zhu, S.-H.; Öttinger, H. C. *J. Rheol.* **1999**, *43*, 795.
(16) Rothstein, J. P.; McKinley, G. H. *J. Non-Newton. Fluid Mech.* **2002**, *108*, 275.
(17) Le Meins, J. F.; Tassin, J. F.; Corpart, J. M. *J. Rheol.* **1999**, *43*, 1423.

(18) Le Meins, J. F. PhD Thesis, Faculté des Sciences, Université Du Maine, 2000.
(19) Pellens, L.; Ahn, K. H.; Lee, S. J.; Mewis, J. *J. Non-Newton. Fluid Mech.* **2004**, *121*, 87.
(20) Vaccaro, A.; Marrucci, G. *J. Non-Newton. Fluid Mech.* **2000**, *92*, 261.
(21) Wetzel, W. H.; Chen, M.; Glass, J. E. Hydrophilic Polymers; *Adv. Chem. Ser.* **1996**, *248*, 163.
(22) Pellens, L. PhD Thesis, Faculteit Toegepaste Wetenschappen, K.U. Leuven, 2004.
(23) Macosko, C. W. *Rheology: Principles, Measurements, and Applications*; Wiley-VCH: New York, 1994.
(24) Burghardt, W. R.; Fuller, G. G. *J. Rheol.* **1989**, *33*, 771.
(25) Zhang, Q.; Archer L. A. *Macromolecules* **2004**, *37*, 1928.
(26) Mewis, J.; Kaffashi, B.; Vermant, J.; Butera, R. J. *Macromolecules* **2001**, *34*, 1376.
(27) English, R. J.; Gulati, H. S.; Jenkins, R. D.; Khan, S. A. *J. Rheol.* **1997**, *41*, 427.
(28) Baravian, C.; Quemada, D. *Rheol. Acta* **1998**, *37*, 223.
(29) Copic, M. *J. Chem. Phys.* **1957**, *26*, 1382.
(30) François, J.; Maitre, S.; Rawiso, M.; Sarazin, D.; Beinert, G.; Isel, F. *Colloids Surf. A: Physicochem. Eng. Asp.* **1996**, *112*, 251.
(31) Hamley, I. W. *J. Phys.: Condens. Matter* **2001**, *13*, R643.
(32) Mortensen, K.; Theunissen, E.; Kleppinger, R.; Almdal, K.; Reynaers, H. *Macromolecules* **2002**, *35*, 7773.
(33) Warner, H. R. *Ind. Eng. Chem. Fundam.* **1972**, *11*, 379.
(34) Green, M. S.; Tobolsky, A. V. *J. Chem. Phys.* **1946**, *14*, 80.
(35) Kuhn, W.; Grün, F. *Kolloid-Z.* **1942**, *101*, 248.
(36) Treloar, L. R. G. *The Physics of Rubber Elasticity*; Clarendon: New York, 1975.
(37) Schröder, U. P.; Oppermann, W. *Makromol. Chem. Macromol. Symp.* **1993**, *76*, 63.
(38) Alami, E.; Almgren, M.; Brown, W.; François, J. *Macromolecules* **1996**, *29*, 2229.
(39) Kataoka, T.; Kitano, M.; Sasahara, M.; Nishijima, K. *Rheol. Acta* **1978**, *17*, 149.
(40) Ohl, N.; Gleissle, W. *J. Rheol.* **1993**, *37*, 381.
(41) Gourier, C.; Beaudoin, E.; Duval, M.; Sarazin, D.; Maitre, S.; François, J. *J. Colloid Interface Sci.* **2000**, *230*, 41.
(42) Wang, Y. C.; Winnik, M. A. *Langmuir* **1990**, *6*, 1437.
(43) Yekta, A.; Duhamel, J.; Adiwidjaja, H.; Brochard, P.; Winnik, M. A. *Langmuir* **1993**, *9*, 881.
(44) Hulden, M. *Colloids Surf. A: Physicochem. Eng. Asp.* **1994**, *82*, 263.
(45) Beaudoin, E.; Borisov, O.; Lapp, A.; Billon, L.; Hiorns, R. C.; François, J. *Macromolecules* **2002**, *35*, 7436.
(46) Beaudoin, E.; Hiorns, R. C.; Borisov, O.; François, J. *Langmuir* **2003**, *19*, 2058.
(47) Yekta, A.; Xu, B.; Duhamel, J.; Adiwidjaja, H.; Winnik, M. A. *Macromolecules* **1995**, *28*, 956.
(48) Tanaka, F.; Edwards, S. F. *J. Non-Newton. Fluid Mech.* **1992**, *43*, 247.

MA047672K